chemistry proceedings

MDPI

Proceeding Paper

Microwave Irradiation-Assisted Synthesis of Bismuth Ferrite Nanoparticles: Investigating Fuel-to-Oxidant Ratios †

Fatemeh Shahrab and Azadeh Tadjarodi *

Laboratory of Inorganic Materials Synthesis, Department of Chemistry,
Iran University of Science and Technology (IUST), Tehran 16846-13114, Iran; email1@email.com (F.S.)
* Correspondence: tajarodi@iust.ac.ir; Tel.: +98-21-77240517; Fax: +98-21-77491204
† Presented at the 27th International Electronic Conference on Synthetic Organic Chemistry (ECSOC-27), 15–30 November 2023; Available online: https://ecsoc-27.sciforum.net/.

Abstract: Bismuth ferrite, $BiFeO_3$, a multiferroic perovskite oxide, has gained significant attention in the field of materials science due to its unique combination of ferroelectric and antiferromagnetic properties. This inherent dual nature makes it essential for various cutting-edge technologies, including non-volatile memories, spintronics, and energy harvesting devices. However, realizing its full potential requires the precise synthesis of high-purity bismuth ferrite nanoparticles. In this scholarly endeavor, we present a comprehensive exploration of the meticulous fabrication of bismuth ferrite nanoparticles using a microwave-assisted combustion method conducted in the solid-state regime. We utilized bismuth nitrate and iron nitrate as precursor materials, combined with an organic fuel amalgam consisting of ammonium nitrate and glycine. Achieving complete combustion through microwave irradiation required a detailed optimization process for the oxidant-to-fuel ratio and absolute quantities. Our research systematically investigated various fuel-to-oxidant ratios, including 1:1, 3:6, 6:3, and 12:12, all conducted under rigorously controlled microwave irradiation conditions. Subsequent characterization through infrared spectroscopy (IR), X-ray diffraction (XRD), and scanning electron microscopy (SEM) confirmed the successful synthesis of high-purity bismuth ferrite nanoparticles. Furthermore, optimizing the synthesis conditions resulted in nanoparticles with superior purity and structural integrity. In conclusion, we meticulously evaluated the photocatalytic properties of the synthesized bismuth ferrite nanoparticles, with a specific focus on their effectiveness in degrading malachite green. Our findings highlight the significant impact of carefully tailored combustion parameters on the photocatalytic performance of bismuth ferrite nanoparticles, positioning them as promising candidates for various environmental remediation and catalytic applications. This study advances our understanding of the custom synthesis of advanced photocatalytic materials, potentially fostering sustainable technological advancements.

Keywords: Bismuth ferrite; Microwave-assisted combustion method; Photocatalytic properties

Citation: Shahrab, F.; Tadjarodi, A. Microwave Irradiation-Assisted Synthesis of Bismuth Ferrite Nanoparticles: Investigating Fuel-to-Oxidant Ratios. *Chem. Proc.* **2023**, *14*, x. https://doi.org/10.3390/xxxxx

Academic Editor(s):

Published: 15 November 2023

1. Introduction

Microwave-assisted nanoparticle synthesis represents a compelling paradigm shift within the field, driven by the remarkable attributes of microwave irradiation as a potent energy source. Microwave waves, characterized by their high-frequency electromagnetic nature, efficiently couple with polar molecules and dipolar substances, promoting rapid and uniform heating. This property is instrumental in the controlled and precise generation of nanoparticles, in stark contrast to conventional methods, which often exhibit erratic reaction kinetics, temperature gradients, and long reaction durations [1,2]. In the context of nanoparticle synthesis, the employment of microwaves offers several distinctive advantages. One of the primary benefits is the marked reduction in reaction time, as microwave irradiation promotes rapid nucleation and growth processes, facilitating the

production of nanoparticles in a matter of minutes, as opposed to hours or days using traditional methods. Furthermore, the homogeneous distribution of microwave energy throughout the reaction vessel minimizes temperature gradients, yielding nanoparticles with superior size uniformity and crystallinity. This spatially and temporally precise energy delivery allows for the production of nanoparticles with finely tailored properties, which are often challenging to achieve with conventional methods [3–5]. Additionally, the use of microwave waves in nanoparticle synthesis aligns with green and sustainable chemistry principles. The energy-efficient nature of microwave irradiation not only decreases reaction times but also reduces the overall energy consumption, contributing to the eco-friendly synthesis of nanoparticles. Moreover, the decreased reliance on hazardous reagents and solvents, coupled with minimized waste generation, further underscores the environmental benefits of this method. The advantages of microwave-assisted nanoparticle synthesis have catalyzed a prolific surge in scientific investigations aimed at to explore this methodology's full potential. Researchers from diverse disciplines are harnessing microwave irradiation to synthesize nanoparticles with tailored sizes, shapes, and compositions, ultimately broadening the horizons of nanotechnology and its application [6–8].

Among the types of nanoparticles, Bismuth ferrite nanoparticles($BiFeO_3$), represent a captivating focal point in academic and scientific research due to their intricate structural, electrical, magnetic, and optical properties. These nanoparticles adopt a rhombohedral perovskite structure, characterized by specific lattice parameters at room temperature. Significantly, $BiFeO_3$ exhibits concurrent ferroelectric and antiferromagnetic behaviors, marked by a high ferroelectric Curie temperature (TC = 1103 K) and G-type antiferromagnetism with a cycloidal spin structure at the Neel temperature (TN = 643 K) [9,10]. While $BiFeO_3$'s exceptional characteristics hold considerable promise, it is imperative to acknowledge persistent challenges, chiefly its low insulation resistance attributable to oxygen vacancies and the reduction of Fe^{3+} to Fe^{2+}. These challenges necessitate ongoing research endeavors to optimize the material's multifunctionality [11–14]. $BiFeO_3$ nanoparticles have garnered attention in memory devices, energy storage systems, supercapacitors, sensors, and particularly in photocatalysis, where their unique attributes facilitate the degradation of organic pollutants. Hence, the scientific significance of $BiFeO_3$ is firmly rooted in the relentless pursuit of advancing our comprehension of these multifunctional nanoparticles and harnessing their capabilities for theoretical and practical advancements in numerous research arenas [15,16]. The synthesis of $BiFeO_3$ nanoparticles encompasses an array of techniques, including solid-state reactions [17], coprecipitation [18], wet chemical route [19], microemulsion technique [20], hydrothermal route [21], sol-gel process [22], auto-combustion route [23], sono-synthesis [24], Pechini method [25], microwave [26] and others [27]. These techniques have been meticulously scrutinized and enhanced to produce of $BiFeO_3$ nanostructures with tailored properties suited for diverse applications.

In this study, Microwave-assisted combustion synthesis has emerged as innovative method, significantly revolutionizing the preparation of bismuth ferrite ($BiFeO_3$) possessing desirable attributes tailored for diverse applications. This methodology judiciously optimizes the reaction conditions and the molar ratios of fuel precursors and ammonium nitrate, an organic combustion-sustaining agent, to achieve a highly efficient fabrication of high-quality $BiFeO_3$ nanostructures. The application of microwave irradiation imparts several advantageous features, notably encompassing reduced reaction durations and energy-efficient processes, thereby rendering it an eco-friendly approach for synthesizing $BiFeO_3$, as evidenced by previous studies [28]. The efficient synthesis of $BiFeO_3$ via microwave-assisted combustion signifies a groundbreaking stride in environmental research. Specifically, it has the potential to address the pressing issues emanating from the presence of organic dye pollutants in water bodies. $BiFeO_3$, distinguished by its multifaceted attributes, encompassing multiferroic and photocatalytic properties, emerges as a promising agent for eradicating pernicious dyes present in wastewater. The purpose of this article is to investigate the ratio of fuel to oxidant in the process of synthesis of bismuth

ferrite particles by microwave-assisted combustion method conducted in the solid state.

2. Experimental

2.1. Materials

In this study, a set of chemical reagents were utilized: Bismuth (III) nitrate pentahydrate and Iron (III) nitrate nonahydrate as precursors, and Glycine as fuel components and the oxidant employed was Ammonium nitrate, that all of were procured from Merck, a reputable company, with a stated purity > 98%. For microwave absorption, commercial-grade CuO with a purity of 95% was used, which was from Sahand Petroplastic International Co. located in Iran. As a model dye pollutant, Malachite Green was chosen, and it was sourced from commercial suppliers. Sample preparation involved the use of 96% ethanol and distilled water. All the materials were used without further purification, as received from the respective suppliers.

2.2. Characterization and Equipments

The samples were subjected to various analytical techniques for the identifying of functional groups and characterization. Fourier Transform Infrared Spectroscopy (FT-IR) was employed with the KBr pellet technique, using a Shimadzu spectrometer operating within the range of 400–4000 cm^{-1}. Powder X-ray Diffraction (PXRD) patterns were acquired using a Bruker D8 Advance diffractometer, utilizing Cu Kα radiation (λ = 1.54060 Å), with using XPERT software. Scanning Electron Microscopy (SEM) was conducted using a VEGA\TESCAN S360 instrument equipped with a backscattered electron detector, and the samples were sputter-coated with gold before imaging. Additionally, Fisher Scientific FB15047 Heated Ultrasonic Bath was utilized. The investigation of photocatalytic properties concerning malachite green was carried out using UV-Vis Shimadzu Series 1700 and mercury lamp spectroscopy.

2.3. Synthesis Method

Synthesis of $BiFeO_3$ nanoparticles: In the synthesis of $BiFeO_3$ nanopowder via the microwave-assisted combustion solid-state route, we employed analytical-grade starting materials, specifically bismuth nitrate pentahydrate [$Bi(NO_3)_3{\cdot}5H_2O$] and iron (III) nitrate nonahydrate [$Fe(NO_3)_3{\cdot}9H_2O$] in a 1:1 molar ratio. To be precise, we utilized one mmol of iron (III) nitrate nonahydrate (equal to 0.404 g) and one mmol of bismuth nitrate pentahydrate (equal to 0.485 g). For the fuel and oxidant components, glycine was employed as the fuel source, and ammonium nitrate was chosen as the oxidizing agent. We investigated various ratios of fuel to oxidant, including 1:1, 3:6, 6:3, and 12:12, to optimize the reaction conditions.

The synthesis process commenced by mixing these materials meticulously within a small porcelain crucible. Subsequently, the resulting mixture was carefully transferred into a larger porcelain crucible, which was pre-loaded with CuO powder. This thoughtfully designed arrangement, encompassing the selection of materials and their systematic transfer, is of paramount importance for the successful synthesis of $BiFeO_3$ nanopowder using the microwave-assisted combustion solid-state route. Copper oxide plays a pivotal role in this synthesis method. Copper oxide is a proficient absorber of microwave radiation, which is the driving force behind the rapid and controlled formation of $BiFeO_3$ nanoparticles. When exposed to microwave radiation, copper oxide efficiently absorbs and converts electromagnetic energy into thermal energy. This absorbed energy is then utilized to heat the reaction mixture, thereby increasing the reaction kinetics. Without copper oxide, the microwave radiation would be scattered within the reaction chamber, leading to a significantly slower reaction rate and less precise control over particle size and morphology. By enveloping the smaller crucible containing the reactants within a larger crucible filled with copper oxide, the microwave-absorbing properties of CuO are harnessed to their fullest extent. This arrangement ensures that the microwave radiation is efficiently

focused on the reaction mixture, intensifying the heating process and promoting the formation of $BiFeO_3$ nanoparticles. This uniform heating is critical for controlling the size, structure, and properties of the nanoparticles. The quantity of copper oxide used depends on the specific reaction parameters and crucible geometry. In this experimental context, approximately 10 g of copper oxide have been utilized. The synthesis method of nanoparticles is visually represented in Scheme 1. Subsequently, the prepared mixture was placed in a conventional domestic microwave oven operating at a power level of 360 W for 20 min. After this microwave treatment, the resulting product underwent a meticulous cleansing process using distilled water and ethanol. Following the rinsing, the product was subjected to sonication for 5 min in distilled water, utilizing the Fisher Scientific FB15047 Heated Ultrasonic Bath. Finally, the product was dried at 70 °C to obtain the desired nanoparticles.

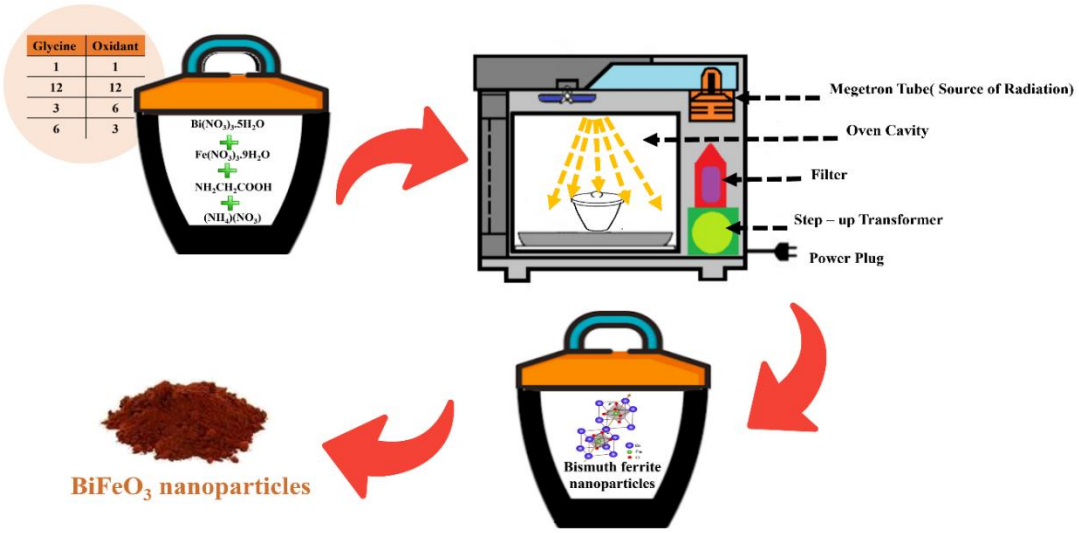

Scheme 1. Illustration for the synthesis of $BiFeO_3$ nanoparticles.

2.4. Photocatalysis Performance

The photocatalytic behavior of bismuth ferrite nanoparticles was assessed through an experimental procedure. As outlined in Scheme 2, a 25 mL aqueous suspension containing the Malachite Green pollutant at a concentration of 10 ppm was prepared. To this suspension, 0.025 g of $BiFeO_3$ nanoparticles was added. The suspension was placed in a reactor and subjected to magnetic stirring. After an initial equilibration period of one hour in complete darkness, the mixture was exposed to visible light emitted by a mercury lamp. Throughout the photocatalytic process, samples were collected at specific time intervals to analyze the progression of the reaction. UV-Vis absorption spectroscopy was utilized to monitor and measure the changes in the adsorption process, providing valuable insights into the effectiveness of the bismuth ferrite nanoparticles as a photocatalyst for degrading the Malachite Green pollutant in UV-visible light.

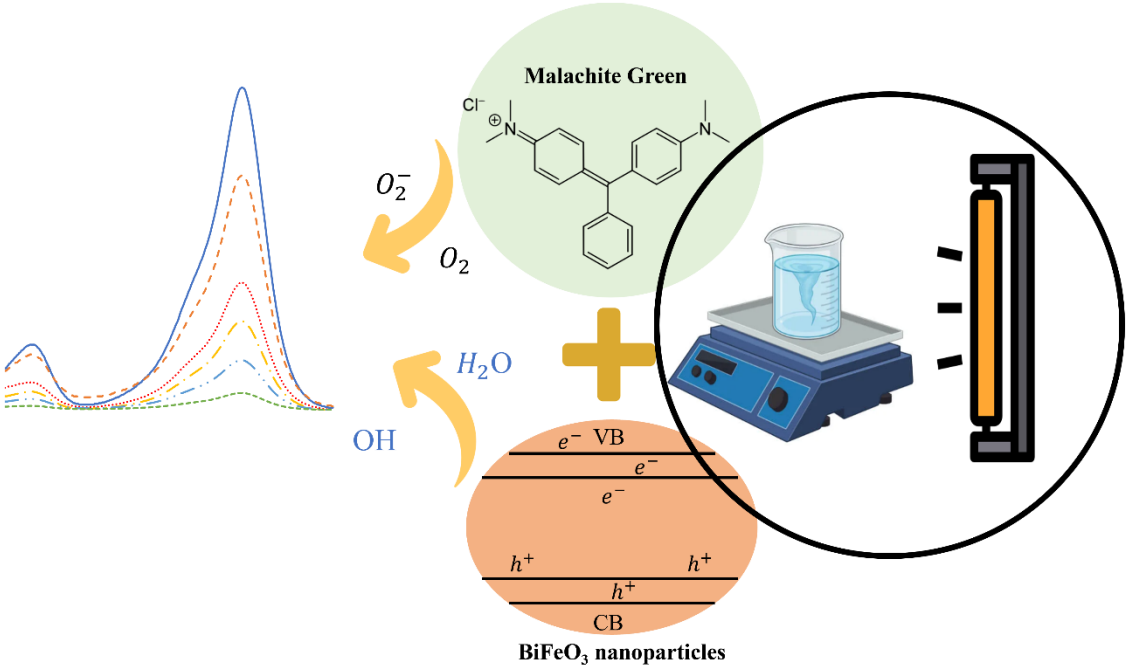

Scheme 2. Illustrate the photocatalytic degradation of Malachite Green by $BiFeO_3$ nanoparticles.

3. Results and discussion

3.1. Characterization of $BiFeO_3$

The product, $BiFeO_3$, underwent comprehensive characterization using FT-IR, XRD, and SEM techniques. In this synthesis method, the complete and optimal combustion of glycine, in combination with ammonium nitrate as the oxidant, plays a pivotal role.

IR: FT-IR analysis is a powerful tool for identifying functional groups in both inorganic and organic compounds. In this study, it was utilized to examine the combustion process of glycine and the synthesis of bismuth ferrite nanoparticles. The FT-IR spectra offered valuable insights into the quality of the nanoparticle synthesis, with sharper and more pronounced peaks in the functional groups of the bismuth ferrite nanoparticles indicating an improved synthesis process.

In the IR spectrum of $BiFeO_3$, two significant bands were identified. One prominent peak appeared at 560 cm^{-1}, attributed to Fe–O stretching, while another was observed at 440 cm^{-1}, related to O–Fe–O vibrations of FeO_6 groups within the perovskite compounds [29].

The infrared spectrum of glycine provides critical insights into its molecular composition and structural characteristics. Several significant peaks in the spectrum correspond to distinct functional groups and vibrational modes within the glassine molecule. Among these, the peak at 3414 cm^{-1} is attributed to the Asymmetrical NH_2 stretch, indicating the stretching vibrations of amino (NH_2) groups. Peak 3084 cm^{-1} represents the Asymmetrical CH stretch, signifying the stretching vibrations of asymmetrical CH (methylene) groups. At 2920 cm^{-1}, the Symmetrical CH stretch is evident, reflecting the symmetrical stretching vibrations of CH groups. The peak at 1703 cm^{-1} is associated with the C=O stretch, in addition to other vibrations, denoting the presence of carbonyl (C=O) functional groups along with other molecular vibrations. Moreover, the 1610 cm^{-1} peak corresponds to NH_2 scissoring, indicating the scissoring motion of NH_2 groups, while the 1410 cm^{-1} peak is related to CH_2 scissoring, representing the scissoring vibrations of CH_2 groups. Lastly, the peak at 584 cm^{-1} is associated with COOH bending, signifying the bending vibrations of carboxylic acid (COOH) functional groups [30].

Additionally, the infrared spectrum of ammonium nitrate reveals distinctive peaks at 1380 and 826 cm^{-1}, further contributing to the comprehensive characterization of these compounds and their unique vibrational modes [31].

Figure 1 illustrates the FT-IR spectrum of different ratios of glycine to ammonium nitrate. Notably, when the ratio of fuel to oxidant was 1:1, there were no observable peaks indicative of the synthesis of bismuth ferrite nanoparticles. This suggests that the quantities of glycine and ammonium nitrate were insufficient compared to the raw materials. Using a ratio of 12:12, though weak bismuth ferrite peaks were present, numerous impurity peaks emerged, likely associated with the formation of impurities such as Bi_2Fe4O_9 and Bi_2FeO_{34}. Additionally, peaks linked to glycine and ammonium nitrate were prominent, indicating an excessive amount of these components relative to the raw materials. In the subsequent step, a ratio of 3 moles of oxidant to 6 moles of glycine was chosen. In this configuration, the peaks corresponding to bismuth ferrite nanoparticle synthesis were visible, and the undesired impurity peaks were minimized. The peaks associated with glycine were present in reduced amounts, and no peaks from ammonium nitrate were observed. This suggested that the quantity of oxidant was lower than that of the fuel in the combustion process, leaving some glycine in the final composition. Finally, 6 moles of oxidant to 3 moles of glycine was selected as the optimal ratio. In this case, the synthesis peaks of bismuth ferrite nanoparticles were well-defined, impurity peaks were absent, and the presence of glycine and ammonium nitrate peaks was significantly reduced. Consequently, this ratio was deemed ideal for the synthesis process.

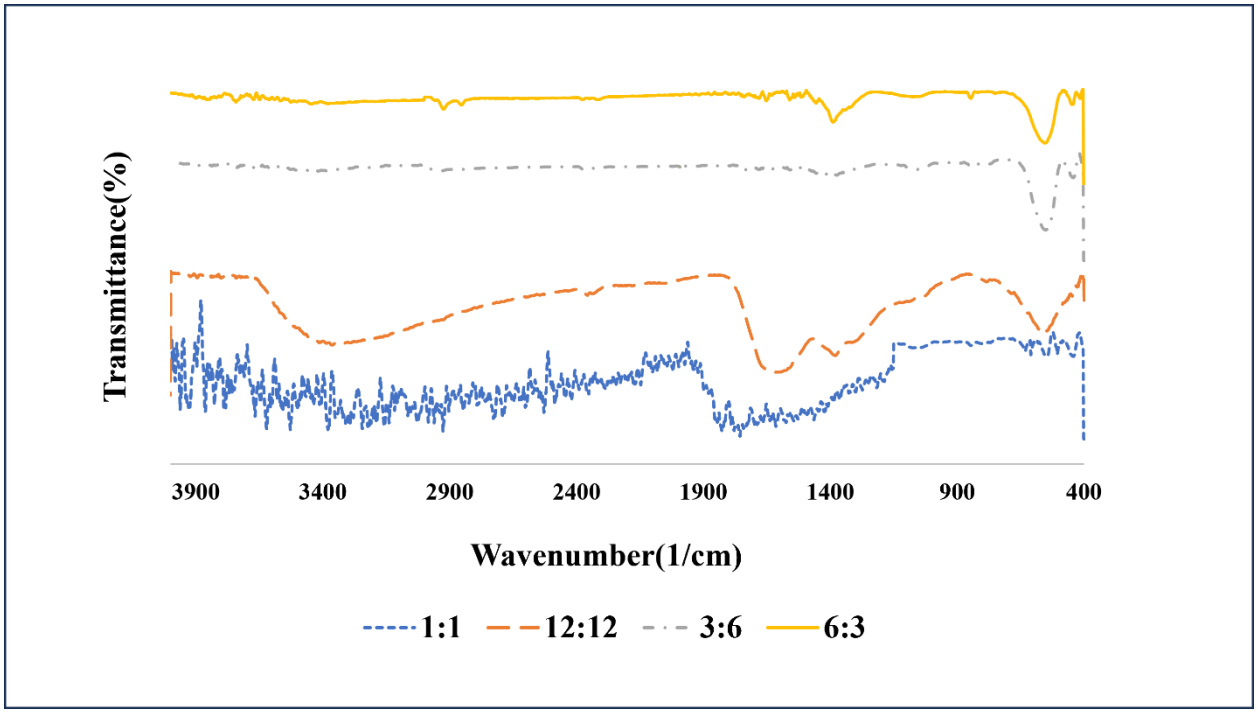

Figure 1. FT-IR spectra of the prepared bismuth ferrite nanoparticles with the different ratio Fuels:Oxidant.

XRD: In Figure 2, the X-ray Diffraction (XRD) pattern is utilized to investigate the impact of varying the fuel ratio on the synthesis of bismuth ferrite nanoparticles. The distinct diffraction peaks at different 2Θ values and their corresponding intensities provide valuable information about the crystallographic structure of the synthesized nanoparticles. By comparing the XRD patterns at different fuel ratios, one can discern changes in peak positions and intensities, which are indicate variations in the crystal structure and purity of the resulting nanoparticles.

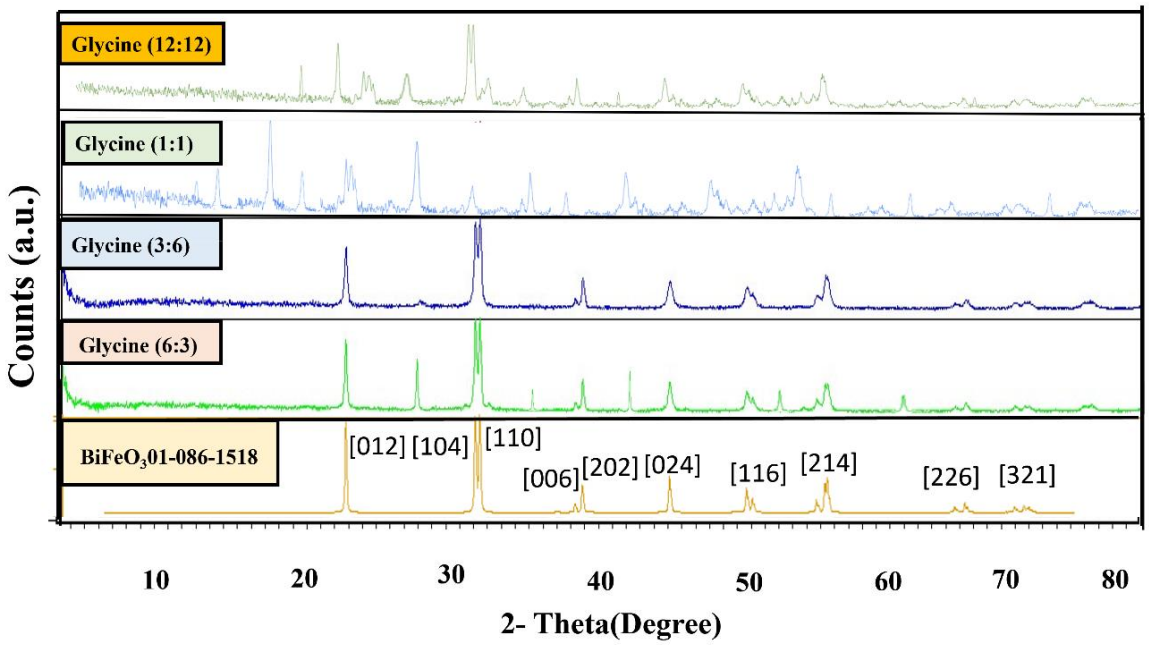

Figure 2. XRD patterns of $BiFeO_3$ nanoparticles with the different ratio Fuels:Oxidant.

The crystallographic data nanoparticles $BiFeO_3$ f the resulting compound exhibited a high degree of conformity with ASTM card No. 01-086-1518. The XRD pattern revealed distinct diffraction peaks at various 2Θ values, signifying the presence of specific crystallographic planes. Notably, the diffraction peaks at 2Θ values of 22.41°, 31.75°, 32.06°, 38.95°, 39.48°, 45.45°, 50.37°, 51.31°, 51.73°, 56.36°, 56.96°, 66.34°, and 67.06° corresponded to crystallographic planes (012), (104), (110), (006), (202), (024), (211), (116), (122), (018), (214), (208), and (220), respectively[32].

These peaks indicate the presence of well-defined crystalline facets in the synthesized $BiFeO_3$ compound. The X-ray Diffraction (XRD) pattern analysis underscores the significant impact of the fuel-to-oxidant ratio on the synthesis of bismuth ferrite nanoparticles. At a 1:1 ratio, there is a conspicuous absence of the characteristic peaks associated with bismuth ferrite nanoparticles, while impurity peaks, predominantly corresponding to bismuth oxide and iron oxide, are prominently evident. The 12:12 ratio exhibits peaks linked to iron oxide, bismuth oxide, and the impurities Bi_2FeO_{34} and $Bi_2Fe_4O_9$.

However, at the 6:3 ratio, the XRD pattern reveals peaks indicative of bismuth ferrite nanoparticles, alongside impurities such as bismuth oxide and $Bi_2Fe_4O_9$. It is noteworthy that the optimal ratio for synthesizing bismuth ferrite nanoparticles appears to be 3:6. In this configuration, the XRD pattern displays bismuth ferrite peaks with high intensity. In contrast, the impurity peaks associated with bismuth oxide are minimized, resulting in a product of the highest quality.

This comprehensive exploration of different fuel-to-oxidant ratios underscores the pivotal role of this parameter in governing the composition and purity of the synthesized bismuth ferrite nanoparticles. Ultimately, it leads to the identifying the ideal ratio for achieving high-quality, pure nanoparticles with enhanced crystallinity.

SEM: The morphological analysis, as depicted in Figure 3, affords valuable insights into the intricate interrelationship between fuel selection and resultant particle dimensions during the preparatory process. These visual representations unveil the presence of discrete, spongy, eliciting heightened scientific curiosity. Augmenting this curiosity is the remarkable homogeneity characterizing their distribution throughout the specimen. Furthermore, these micrographs elucidate the intriguing presence of voids within the structural constitution of these particles. This empirical observation clarifies the fundamental

correlation between the specific fuel-to-oxidant ratio employed and the consequent attributes of the synthesized particles. The consistent dissemination of frothy particles implies that precise fuel-to-oxidant ratios may foster uniform nucleation and growth, culminating in a meticulously controlled particle size distribution. Additionally, identifying voids within the particles alludes to the potential for gaseous evolution or the involvement of volatile constituents during the synthesis procedure.

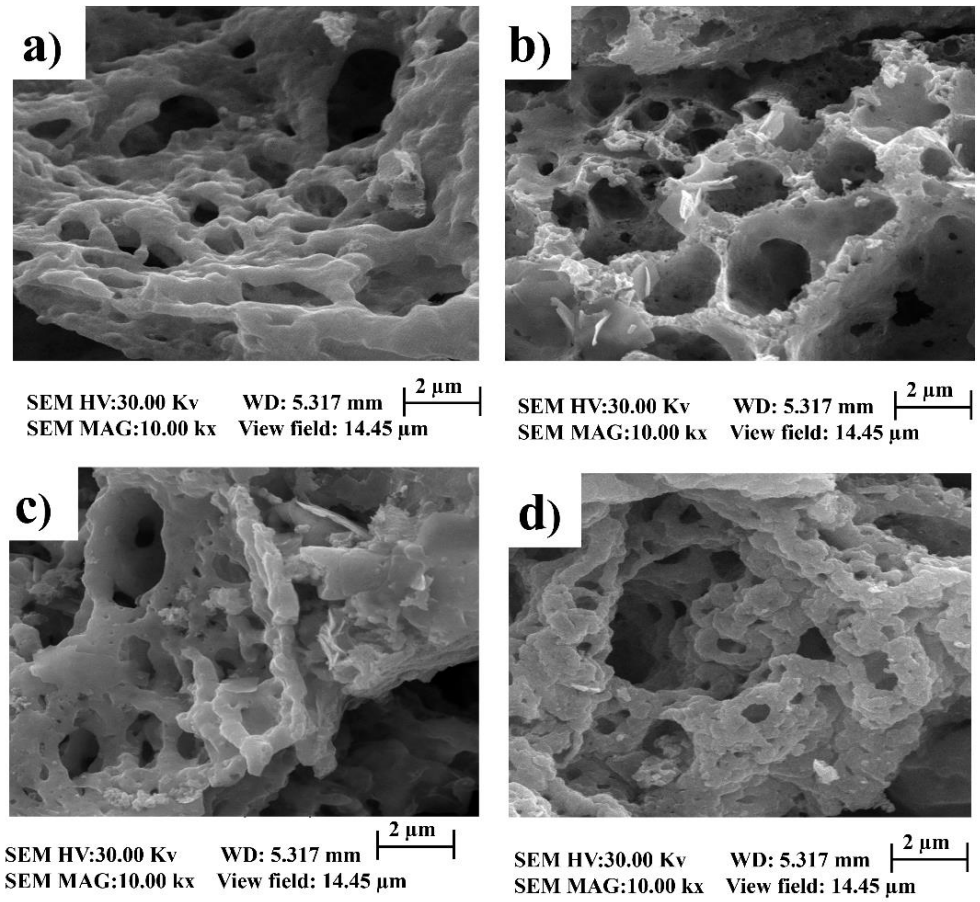

Figure 3. SEM images of $BiFeO_3$ nanoparticles with different ratio Fuels:Oxidant.

3.2. Photocatalytic Behavior of Nanoparticles $BiFeO_3$

To confirm the photocatalytic properties, precisely 0.025 g of bismuth ferrite, synthesized at a specific 3:6 ratio, were meticulously introduced into the reaction vessel alongside Malachite green. The UV-Vis spectrum of Malachite green, with an initial concentration of 10 ppm, was closely monitored at different time intervals, as depicted in Figure 4.

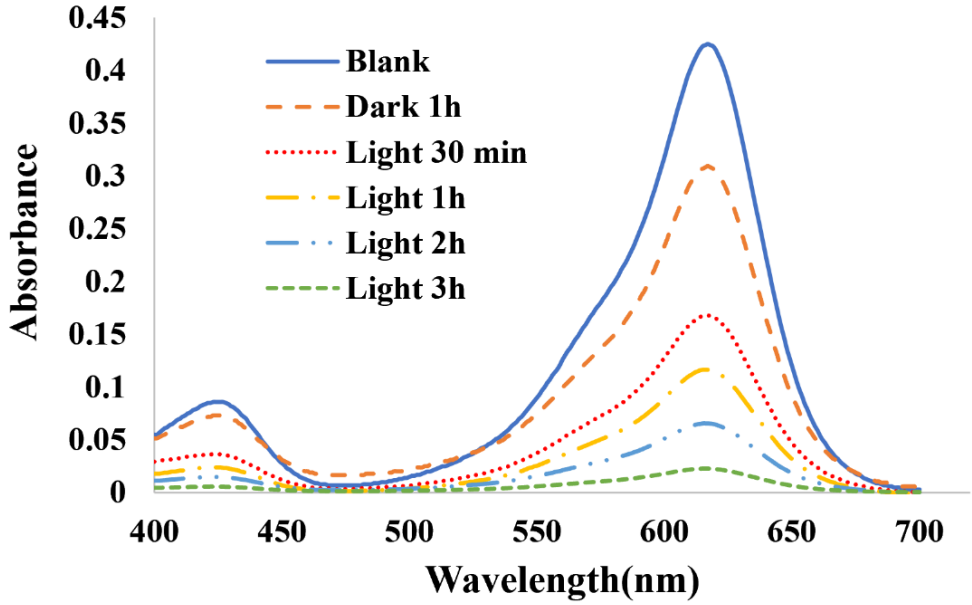

Figure 4. UV–Vis spectra of 10 ppm concentration Malachite Green.

In the context of studying photocatalysis, the percentage of pollutant decolorization in water was quantified using a well-defined Equation (2) [29]:

$$C_t = (A_1 \times C_0)/A_0 \quad (2)$$

Here, C_0 signifies the initial concentration, while C_t denotes the concentration at the specific moment of interest. A_1 quantifies the current level of adsorption, while A_0 represents the initial concentration of the pollutant. The tabulated data in Table 1 provides a comprehensive overview of the pollutant decomposition percentages observed at various time intervals.

Table 1. The degradation percentage of Malachite Green.

Catalyst	Degradation (%) 30 min	Degradation (%) 60 min	Degradation (%) 120 min	Degradation (%) 180 min
$BiFeO_3$	60.47	72.70	84.62	96.86

The degradation percentage was calculated with reference to the initial concentration (C_0), which was determined after a one-hour dark exposure. A comprehensive kinetic analysis was conducted to identify the most suitable kinetic model governing the photocatalytic decomposition of Malachite green over 180 min, as visually represented in Figure 5. The pseudo-first-order kinetics model can be mathematically expressed as follows (Equation (3)) [33]:

$$\ln(C_0/C_t) = K_{app} \times t \quad (3)$$

Here, C_0 represents the initial dye concentration (mg/L), C_t reflects the dye concentration during the specified time interval (mg/L), K_{app} characterizes the apparent reaction rate constant (min^{-1}), and t accounts for the elapsed reaction time (minutes). The dominant mechanism responsible for the photocatalytic decomposition was attributed to the notably short half-life of the oxidizing radicals, whose concentrations remained presumed to be constant, albeit unidentifiable and unmeasurable at specific time points.

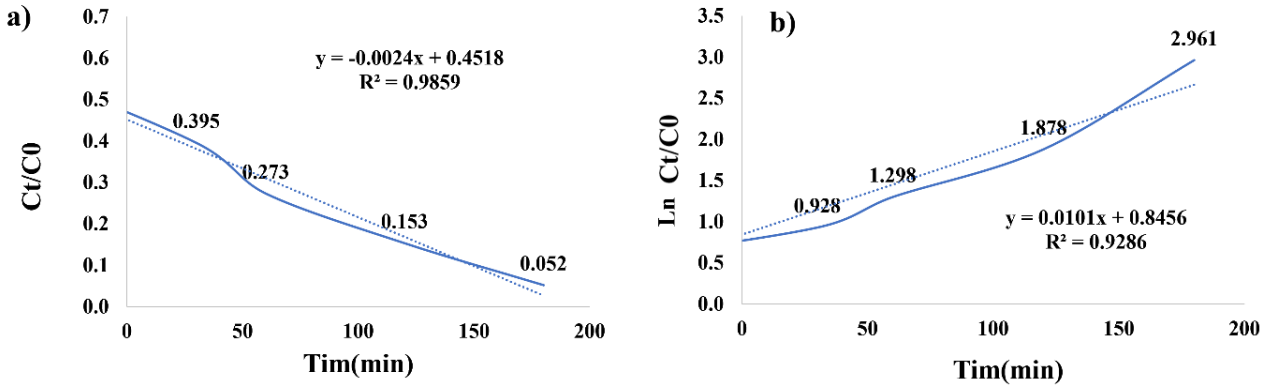

Figure 5. Photocatalytic degradation and rate (**a**), Kinetics degradation Malachite Green (**b**).

4. Conclusions

The synthesis of $BiFeO_3$ nanoparticles through the microwave-assisted combustion solid-state route involves a systematic selection of precursor materials, fuel, and fuel-oxidant ratios, significantly shaping the resulting material. The IR spectrum effectively identifies the functional groups involved in the combustion process of glycine and the synthesis of bismuth ferrite nanoparticles. This analytical technique highlights the peaks associated with bismuth ferrite nanoparticles and the composition of glycine, ammonium nitrate, and fuel. These findings underscore the potential for fine-tuning the synthesis process by optimizing the fuel-to-oxidant ratio to achieve the desired particle size and structural attributes.

The X-ray Diffraction analysis underscored the critical role of the fuel-to-oxidant ratio in controlling the presence of crystalline facets in the synthesized $BiFeO_3$ compound. The 1:1 ratio resulted in pronounced impurity peaks, primarily due to bismuth oxide and iron oxide. In contrast, the 6:3 ratio yielded distinct peaks representing bismuth ferrite nanoparticles and impurities such as bismuth oxide and $Bi_2Fe_4O_9$. The optimal ratio of 3:6 emerged as the ideal choice, characterized by intense bismuth ferrite peaks and minimal impurities, affirming the significance of the fuel-to-oxidant ratio in customizing material properties.

Furthermore, examining the product's morphology provided critical insights into the role of the chosen fuel in determining particle size. The images revealed foamy, agglomerated particles with a consistent distribution and cavities within their structures. This observation unveiled the intricate connection between fuel selection and particle characteristics, highlighting the influence of fuel on nucleation and growth. These findings underscore the potential for fine-tuning the synthesis process by optimizing the fuel-to-oxidant ratio to achieve the desired particle size and structural attributes.

Author Contributions:.

Funding:

Institutional Review Board Statement:

Informed Consent Statement:

Data Availability Statement:

Acknowledgments: We are grateful from Iran University of Science and Technology for providing materials and some facilities.

Conflicts of Interest:

References

1. Kumar, A.; Kuang, Y.; Liang, Z.; Sun, X. Microwave chemistry, recent advancements, and eco-friendly microwave-assisted synthesis of nanoarchitectures and their applications: A review. *Mater. Today Nano* **2020**, *11*, 100076, https://doi.org/10.1016/j.mtnano.2020.100076.
2. Polshettiwar, V.; Nadagouda, M.N.; Varma, R.S. Microwave-assisted chemistry: A rapid and sustainable route to synthesis of organics and nanomaterials. *Aust. J. Chem.* **2009**, *62*, 16–26, https://doi.org/10.1071/ch08404.
3. Becerra-Paniagua, D.K.; Díaz-Cruz, E.B.; Baray-Calderón, A.; Garcia-Angelmo, A.R.; Regalado-Pérez, E.; Rodriguez-Torres, M.d.P.; Martínez-Alonso, C. Nanostructured metal sulphides synthesized by microwave-assisted heating: A review. *J. Mater. Sci. Mater. Electron.* **2022**, *33*, 22631–22667, https://doi.org/10.1007/s10854-022-09024-9.
4. Jadhav, A.; Devale, R.P. Review on Microwave, The General purpose in Microwave Assisted Synthesis for Green Chemistry. *Asian J. Res. Chem.* **2022**, *15*, 182–185, https://doi.org/10.52711/0974-4150.2022.00031.
5. Kaur, N.; Singh, A.; Ahmad, W. Microwave assisted green synthesis of silver nanoparticles and its application: A review. *J. Inorg. Organomet. Polym. Mater.* **2022**, *33*, 663–672, https://doi.org/10.1007/s10904-022-02470-2.
6. Krishnan, R.; Shibu, S.N.; Poelman, D.; Badyal, A.K.; Kunti, A.K.; Swart, H.C.; Menon, S.G. Recent advances in microwave synthesis for photoluminescence and photocatalysis. *Mater. Today Commun.* **2022**, *32*, 103890. https://doi.org/10.1016/j.mtcomm.2022.103890.
7. Diaz de Grenu, B.; de Los Reyes, R.; Costero, A.M.; Amorós, P.; Ros-Lis, J.V. Recent progress of microwave-assisted synthesis of silica materials. *Nanomaterials* **2020**, *10*, 1092.
8. Yadav, A.R.; Mohite, S.K. A brief review: Microwave chemistry and its applications. *Res. J. Pharm. Dos. Forms Technol.* **2020**, *12*, 191–197.
9. Yousaf, M.; Lu, Y.; Hu, E.; Wang, B.; Akhtar, M.N.; Noor, A.; Akbar, M.; Shah, M.Y.; Wang, F.; Zhu, B. Tunable magneto-optical and interfacial defects of Nd and Cr-doped bismuth ferrite nanoparticles for microwave absorber applications. *J. Colloid Interface Sci.* **2021**, *608*, 1868–1881, https://doi.org/10.1016/j.jcis.2021.09.182.
10. Neha, N.; Verma, R.; Chauhan, A.; Kumari, N.; Kumar, P.; Kumar, R. Effect of synthesis techniques on the magnetic properties of Bismuth ferrite: A review. In Proceedings of the AIP Conference Proceedings, Breclavi, Czech Republic, 26–30 May 2022; AIP Publishing LLC: Melville, NY, USA, 2022; Volume 2357.
11. Aepuru, R.; Kumar, V.; Verma, P.; Sahoo, P.K.; Panda, H. Polarization Induced Multiferroic Bismuth Ferrite Nanostructures: Investigation of Dielectric and Magnetic Properties. In Proceedings of the 2021 International Scientific Conference Electronics (ET), Sozopol, Bulgaria, 15–17 September 2021; pp. 1–8.
12. Zhang, J.; Cui, Y.; Liu, N.; Qi, Q.; Huang, R.; Chen, K.; Liu, L.; Han, Z.; Yuan, G. Quasipolaron Surface Polarization in Bismuth Ferrite. *Phys. Rev. Appl.* **2022**, *18*, L051002, https://doi.org/10.1103/physrevapplied.18.l051002.
13. Shi, Y.; Yan, F.; He, X.; Huang, K.; Shen, B.; Zhai, J. B-site-doped BiFeO3-based piezoceramics with enhanced ferro/piezoelectric properties and good temperature stability. *J. Am. Ceram. Soc.* **2020**, *103*, 6245–6254.
14. Lacerda, L.H.S.; de Lazaro, S.R. Density Functional Theory investigation of rhombohedral multiferroic oxides for photocatalytic water splitting and organic photodegradation. *J. Photochem. Photobiol. A Chem.* **2020**, *400*, 112656.
15. Ćurković, L.; Veseli, R.; Gabelica, I.; Žmak, I.; Ropuš, I.; Vukšić, M. A review of microwave-assisted sintering technique. *Trans. FAMENA* **2021**, *45*, 1–16.
16. Gao, T.; Chen, Z.; Huang, Q.; Niu, F.; Huang, X.; Qin, L.; Huang, Y. A review: Preparation of bismuth ferrite nanoparticles and its applications in visible-light induced photocatalyses. *Rev. Adv. Mater. Sci.* **2015**, *40*, 97–109.
17. Bak, J.-W.; Ham, Y.-S.; Shin, S.-Y.; Park, K.-J.; You, C.-Y.; Jeong, D.-Y.; Cho, N.-H. Fine Control of Multiferroic Features of Nanoscale BiFeO3 Powders Synthesized by Microwave-Assisted Solid-State Reaction. *Electron. Mater. Lett.* **2023**, *19*, 495–501, https://doi.org/10.1007/s13391-023-00412-9.
18. Sulistiani, F.A.; Suharyadi, E.; Kato, T.; Iwata, S. Effects of NaOH concentration and temperature on microstructures and magnetic properties of bismuth ferrite (BiFeO3) nanoparticles synthesized by coprecipitation method. *Key Eng. Mater.* **2020**, *855*, 9–15, https://doi.org/10.4028/www.scientific.net/kem.855.9.
19. Mukherjee, S. Bandgap and PL Spectra of Bismuth Ferrite-Nickel Ferrite Nanocomposites Synthesized by Wet Chemistry. *Interceram Int. Ceram. Rev.* **2020**, *69*, 50–53, https://doi.org/10.1007/s42411-020-0421-0.
20. Nazeer, Z.; Bibi, I.; Majid, F.; Kamal, S.; Ghafoor, A.; Ali, A.; Kausar, A.; Elqahtani, Z.M.; Alwadai, N.; Iqbal, M. Microemulsion synthesis of Ga and Sr doped $BiFeO_3$ nanoparticles and evaluation of their ferroelectric, optical, dielectric and photocatalytic properties. *Phys. B Condens. Matter* **2023**, *657*, 414788. https://doi.org/10.1016/j.physb.2023.414788.
21. Sanga, P.; Wang, J.; Li, X.; Chen, J.; Qiu, H. Effective Removal of Sulfonamides Using Recyclable MXene-Decorated Bismuth Ferrite Nanocomposites Prepared via Hydrothermal Method. *Molecules* **2023**, *28*, 1541, https://doi.org/10.3390/molecules28041541.
22. Mubarak, T.H.; Hassan, K.H.; Khodair, Z.T.; Kareem, C.H.; Kamil, A.A. Characterization of nanostructured bismuth ferrite (BiFeO3) prepared by sol-gel method. In Proceedings of the 2nd International Conference on Mathematical Techniques and Applications: Icmta2021, Kattankulathur, India, 24–26 March 2021; p. 090022.
23. Mhamad, S.A.; Ali, A.A.; Mohtar, S.S.; Aziz, F.; Aziz, M.; Jaafar, J.; Yusof, N.; Salleh, W.N.W.; Ismail, A.F.; Chandren, S. Synthesis of bismuth ferrite by sol-gel auto combustion method: Impact of citric acid concentration on its physicochemical properties. *Mater. Chem. Phys.* **2022**, *282*, 125983, https://doi.org/10.1016/j.matchemphys.2022.125983.

24. Palomino-Resendiz, R.L.; Bolarín-Miró; AM.; Pedro-García, F.; Sánchez-De Jesús, F.; Espinós-Manzorro, J.P.; Cortés-Escobedo, C.A. Analysis of the effect of cationic ratio Bi3+/Fe3+ on the magnetic and multiferroic properties of $BiFeO_3$ nanoparticles synthesized using a sonochemical-assisted method. *Ceram. Int.* **2022**, *48*, 14746–14753.
25. Parvez, M.M.; et al., Synthesis of Bismuth Ferrite Nanoparticles by Modified Pechini Sol-Gel Method. *Int. J. Sci. Eng. Investig.* **2020**, *9*, 35–38.
26. Banoth, P.; Sohan, A.; Kandula, C.; Kanaka, R.K.; Kollu, P. Microwave-assisted solvothermal route for one-step synthesis of pure phase bismuth ferrite microflowers with improved magnetic and dielectric properties. *ACS Omega* **2022**, *7*, 12910–12921, https://doi.org/10.1021/acsomega.2c00219.
27. S., D.; Tayade, R.J. Low temperature energy- efficient synthesis methods for bismuth-based nanostructured photocatalysts for environmental remediation application: A review. *Chemosphere* **2022**, *304*, 135300, https://doi.org/10.1016/j.chemosphere.2022.135300.
28. Shahrab, F.; Tadjarodi, A. Exploring the role of fuel in the synthesis of bismuth ferrite nanoparticles by microwave-assisted combustion in solid state and the study of photocatalytic degradation of Brilliant Blue. *J. Mol. Struct.* **2024**, *1295*, 136806. https://doi.org/10.1016/j.molstruc.2023.136806.
29. Nazir, A.; Latif, S.; Adil, S.F.; Kuniyil, M.; Imran, M.; Hatshan, M.R.; Kanwal, F.; Shaik, B. Photocatalytic Degradation of Cefixime Trihydrate by Bismuth Ferrite Nanoparticles. *Materials* **2021**, *15*, 213, https://doi.org/10.3390/ma15010213.
30. Kumar, S.; Rai, A.K.; Singh, V.B.; Rai, S.B. Vibrational spectrum of glycine molecule. *Spectrochim. Acta Part A Mol. Biomol. Spectrosc.* **2005**, *61*, 2741–2746.
31. Kubota, H.; Liu, C.; Toyao, T.; Maeno, Z.; Ogura, M.; Nakazawa, N.; Inagaki, S.; Kubota, Y.; Shimizu, K.I. Formation and reactions of NH_4NO_3 during transient and steady-state NH3-SCR of NO x over H-AFX zeolites: Spectroscopic and theoretical studies. *ACS Catal.* **2020**, *10*, 2334–2344.
32. Wu, S.; Zhang, J.; Liu, X.; Lv, S.; Gao, R.; Cai, W.; Wang, F.; Fu, C. Micro-area ferroelectric, piezoelectric and conductive properties of single BiFeO3 nanowire by scanning probe microscopy. *Nanomaterials* **2019**, *9*, 190, https://doi.org/10.3390/nano9020190.
33. Nkwachukwu, O.V.; Muzenda, C.; Ojo, B.O.; Zwane, B.N.; Koiki, B.A.; Orimolade, B.O.; Nkosi, D.; Mabuba, N.; Arotiba, O.A. Photoelectrochemical degradation of organic pollutants on a La3+ doped BiFeO3 perovskite. *Catalysts* **2021**, *11*, 1069.